9-1-2009

Optical Acquisition and Polar Decomposition of the Full-Field Deformation Gradient Tensor Within a Fracture Callus

Wangdo Kim
Portland State University

Sean S. Kohles
Portland State University

Citation Details

Kim, W., & Kohles, S. S. (2009). Optical acquisition and polar decomposition of the full-field deformation gradient tensor within a fracture callus. Journal Of Biomechanics, 42(13), 2026-2032.

Optical Acquisition and Polar Decomposition of the Full-Field Deformation Gradient Tensor Within a Fracture Callus

Wangdo Kim[1] and **Sean S. Kohles**[1,2,*]

[1] Department of Mechanical & Materials Engineering, Portland State University, Portland, OR, USA

[2] Kohles Bioengineering Portland, OR, USA, and Department of Surgery, Oregon Health & Science University, Portland, OR, USA

Abstract

Tracking tissue deformation is often hampered by material inhomogeneity, so local measurements tend to be insufficient thus lending to the necessity of full-field optical measurements. This study presents a novel approach to factoring heterogeneous deformation of soft and hard tissues in a fracture callus by introducing an anisotropic metric derived from the deformation gradient tensor (**F**). The deformation gradient tensor contains all the information available in a Green-Lagrange strain tensor, plus the rigid-body rotational components. A recent study [Bottlang et al., *J. Biomech.* 41(3), 2008] produced full-field strains within ovine fracture calluses acquired through the application of electronic speckle pattern interferometery (ESPI). The technique is based on infinitesimal strain approximation (Engineering Strain) whose scheme is not independent of rigid body rotation. In this work, for rotation extraction, the stretch and rotation tensors were separately determined from **F** by the polar decomposition theorem. Interfragmentary motions in a fracture gap were characterized by the two distinct mechanical factors (stretch and rotation) at each material point through full-field mapping. In the composite nature of bone and soft tissue, collagen arrangements are hypothesized such that fibers locally aligned with principal directions will stretch and fibers not aligned with the principal direction will rotate and stretch. This approach has revealed the deformation gradient tensor as an appropriate quantification of strain within callus bony and fibrous tissue via optical measurements.

Keywords

1. Introduction

Many studies have demonstrated the importance of interfragmentary strain as a mechanism for controlling fracture healing during the reparative phase in which bone stiffness is restored [Einhorn, 1995; Marsh and Li, 1999]. Interfragmentary strain hypotheses attempt to provide a unifying theory relating controlled fracture loading and mobilization, to the tissue response

---

[Epari et al., 2006]. The concept of defining a global interfragmentary strain associated with fracture healing and callus formation often disregards local tissue heterogeneity. Actual structural and mechanical heterogeneity results in a complex distribution of stress and strain. These localized mechanical conditions guide the differentiation of the various tissue types in fracture callus formation [Claes et al., 1998]. Several mechanoregulation algorithms, proposed to control tissue differentiation during bone healing, have been shown to predict tissue distribution [Isaksson et al., 2006].

Interfragmentary motion of bone fragments have been typically studied by measuring the rigid body movements between bone structures bordering a fracture gap. Examples include: gap displacements monitored with reflective markers [Duda et al., 2002]; interfragmentary displacement in a tibial fracture measured in axial, angular and shear components by using an instrumented spatial linkage [Kenwright, 1998]; interfragmentary sliding (shear) and axial motion associated with healing of a mid-tibial fracture as studied with an electronic motion sensor [Park et al., 1998; Duda et al., 2003]; and relative three-dimensional motion between fracture fragments monitored by an instrumented linkage [Gardner, 1996]. Recently, new tools have been developed for full-field strain measurement taking into account localized heterogeneity of hard and soft tissues. Electronic speckle pattern interferometry (ESPI) is available to measure full-field strain distributions [Erne et al., 2005] and has enabled reproducible quantification of strain distributions within callus cross-sections [Bottlang et al., 2008]. Often strain acquisition approaches are performed via an infinitesimal strain approximation (Engineering Strain) based on the assumption that the examined material experienced only a small change in shape from the reference condition. Most commercially available optical measurement systems are limited to computing strains through displacement gradients only, as this facilitates an expedited analysis by avoiding the generation of the full deformation gradient tensor.

It is hypothesized that the local mechanical environment in a fracture non-union may have distinct components of localized rigid body rotation and deformable stretch in collagen fibers within the interfragmentary region. Fibers aligned with principal directions will only stretch whereas fibers not aligned with the principal direction will both stretch and rotate [Lanir, 1979; Lanir, 1983; Sacks, 2000]. In the present study, a novel method of mapping interfragmentary callus anisotropy is presented by exploiting the deformation gradient tensor and computing localized rigid body rotations as well as stretch deformation in response to uniaxial loading. A detailed map characterizing anisotropy and heterogeneity based on interfragmentary motion within a fracture is presented at resolved material points within a cross-section of a load-bearing callus.

2. Methods

2.1 Estimation of the Deformation Gradient Tensor from Direct Experiments

A theory is presented in which the deformation gradient $\mathbf{F}$ may be computed from the displacements of a discrete set of points, such as an experimentally measured displacement field. The first step in defining large deformation measures is to define the relationship between the reference (initial or undeformed) configuration of a solid surface and the deformed configuration of the analyzed deformable body. The deformation gradient $\mathbf{F}$ is a tensor that quantifies both the two- and three-dimensional (2D and 3D) shape change as well as the overall material rotation [Rodriguez et al., 1994; Cowin, 2004], making it superior to unidirectional strain as an all-encompassing measure of the deformation and kinematics of material elements (Figure 1). Consider an arbitrary fiber or constituent element within an elastic body such as collagen within bone or soft tissue. The physical significance of the deformation gradient is that it relates the deformation vector (magnitude and displacement direction) of an initially

undeformed material fiber **dX** in the reference configuration to the magnitude and direction **dx** in the deformed configuration by a one-to-one mapping function such that:

$$\mathbf{dx} = \mathbf{F} \cdot \mathbf{dX} \tag{1}$$

which results in the deformation tensor at an arbitrary point P:

$$\mathbf{F} = \frac{\partial \mathbf{x}}{\partial \mathbf{X}} \tag{2}$$

The deformed state of the material fiber vector **dx** is neither generally orthogonal nor of unit length.

Consider two neighboring locations, which occupy the points P and Q within the planar continuum at a reference configuration (Figure 1). The coordinates of a group of surface markers including points P and Q are used to determine estimates for the components of **F** at each material point, defined by the centroid of those markers. A computational method based on a Taylor series expansion of a displacement field [Peters, 1987], can directly compute **F** from the experimentally acquired grid pattern displacement field on the surface of a loaded body (here biological). For rotation extraction, the stretch and rotation tensor components are then separated from the **F** tensor by the polar decomposition theorem. The methodology utilizes displacement information produced at discrete points identified on the surface of a loaded body and suitable for biomechanical applications. Methodology beyond that described in the next section is reproduced in the Appendix for completeness.

2.2 Localized Rotation, Principal Stretch Magnitude and Direction

The theory and methodology for decomposing the estimate of **F** ($\hat{\mathbf{F}}$) is based on the assumption that any deformation consists of a combination of a rigid rotation and a deformation or stretch. A rotation is a special kind of deformation in which fiber or elemental constituents permissibly change orientation due to structural anisotropy, of the tissue this case, distinct from any deformation. A stretch is a deformation with vector orientation established in the initial configuration with a magnitude change in length, separate from orientation-only changes.

$\hat{\mathbf{F}}$ may be written as a product of three factors via singular value decomposition (SVD) [Press et al., 1992]:

$$\widehat{\mathbf{F}} = \mathbf{U} \cdot \sum \cdot \mathbf{V^T} \tag{3}$$

In continuum mechanics, this begins to separate the rotation from the stretching components where **U** and **V** are orthogonal stretch matrices (their inverse equals their transpose), and Σ is a diagonal matrix, which are all composed of nonnegative real numbers. For an invertible matrix $\hat{\mathbf{F}}$, there exists a unique orthogonal rotational tensor **R** and a unique symmetric positive definite 'left stretch' tensor **S** such that:

$$\widehat{\mathbf{F}} = \mathbf{S} \cdot \mathbf{R} \tag{4}$$

where $\mathbf{S} = \mathbf{U} \cdot \Sigma \cdot \mathbf{U^T}$ is a symmetric positive semi-definite stretch tensor and $\mathbf{R} = \mathbf{U} \cdot \mathbf{V^T}$ is an orthogonal rotation tensor. Since $\hat{\mathbf{F}} = \mathbf{U} \cdot \Sigma \cdot \mathbf{V^T}$ and $\mathbf{U} \cdot \mathbf{U^T} = \mathbf{I}$ (identity matrix), equation (4) can be confirmed:

$$\widehat{\mathbf{F}} = \mathbf{U} \cdot \sum \cdot (\mathbf{U^T} \cdot \mathbf{U}) \cdot \mathbf{V^T} = (\mathbf{U} \cdot \sum \cdot \mathbf{U^T}) \cdot (\mathbf{U} \cdot \mathbf{V^T}) = \mathbf{S} \cdot \mathbf{R}$$

(5)

The SVD solution, however, sometimes fails to give a correct rotation tensor and gives a reflection instead when the data are severely corrupted. As a check, a least-squares estimation can account for corrupt data and produce the accurate transformation parameters [Umeyama, 1991]:

$$\text{If } |\mathbf{U}| \cdot |\mathbf{V}| > 0, \text{ then } \mathbf{R} = \mathbf{U} \cdot \mathbf{V^T}, \text{ otherwise } \mathbf{R} = \mathbf{U} \cdot \begin{bmatrix} 1 & 0 & 0 \\ 0 & 1 & 1 \\ 0 & 0 & -1 \end{bmatrix} \cdot \mathbf{V^T}.$$

The rotation tensor $\mathbf{R}$ is further characterized by its rotation angle φ about a unique axis of rotation. Eigenvalues of a rotation tensor describe such an angle φ [McCarthy, 2000].

As noted previously, constituent fibers not aligned to principal direction of stretch will rotate φ such that:

$$\varphi = \arccos\left(\frac{\mathbf{R}_{1,1} + \mathbf{R}_{2,2} + \mathbf{R}_{3,3} - 1}{2}\right)$$

(6)

where $\mathbf{R_{i,i}}$ represent the diagonal terms of $\mathbf{R}$ defined during polar decomposition.

Physically, the principal stretch $\mathbf{S}$ describes a deformation in which there is an orthogonal triad of material vectors that change length but not orientation. The principal stretches are determined by taking the eigenvalues of $\mathbf{S}$, which represent the ratios of the deformed length to undeformed length, $\lambda_{\mathbf{i}} = \|\mathbf{x_i}\| / \|\mathbf{X_i}\|$. The corresponding eigenvectors indicate the principal directions of stretch caused by the re-orientation of fibers due to loading (and stretching) along those principal directions. In the absence of material rotation, any material fibers orientated along one of the ith principal stretch directions will not change orientation, but will change length by a factor equal to the designated eigenvalue $\lambda_{\mathbf{i}}$. In the following experimental application, the rotational angles and the principal stretch ratios for stretch at each material point on a loaded callus surface were mapped.

2.3 Green-Lagrange Strain Tensor versus Infinitesimal Strain Tensor

The Green-Lagrange strain tensor $\mathbf{E}$ is related to the previous tensorial descriptions through the following development:

$$\begin{aligned} E_{ij} &= \tfrac{1}{2}\left(\frac{\partial x_k}{\partial X_i}\frac{\partial x_k}{\partial X_j} - \delta_{ij}\right) \\ &= \tfrac{1}{2}(\mathbf{F^T F} - \mathbf{I}) \\ &= \tfrac{1}{2}(\mathbf{FF^T} - \mathbf{I}) = \tfrac{1}{2}((\mathbf{SR})(\mathbf{SR})^T - \mathbf{I}) \\ &= \tfrac{1}{2}(\mathbf{SRR^T S^T} - \mathbf{I}) \\ &= \tfrac{1}{2}(\mathbf{S}^2 - \mathbf{I}) \end{aligned}$$

(7)

in which the final relationship does not depend on the rotational tensor $\mathbf{R}$ and $\mathbf{E}$ is only a function of the stretch tensor $\mathbf{S}$. Since $\mathbf{x} = \mathbf{X} + \mathbf{u}$, where $\mathbf{u}$ is the displacement, $\mathbf{E}$ can be rewritten as:

$$\mathbf{E}=\frac{1}{2}(\frac{\partial \mathbf{u}}{\partial \mathbf{X}}+(\frac{\partial \mathbf{u}}{\partial \mathbf{X}})^{\mathbf{T}}+\frac{\partial \mathbf{u}}{\partial \mathbf{X}}(\frac{\partial \mathbf{u}}{\partial \mathbf{X}})^{\mathbf{T}})$$

(8)

Alternatively, an infinitesimal strain approximation is carried out when the gradient of the displacement can be considered 'small.' In that case, $\mathbf{E}$ reduces to the infinitesimal strain tensor $\mathbf{e}$ by neglecting the higher-order terms of equation (8):

$$\begin{aligned}\mathbf{e}&=\tfrac{1}{2}(\tfrac{\partial \mathbf{u}}{\partial \mathbf{X}}+(\tfrac{\partial \mathbf{u}}{\partial \mathbf{X}})^{\mathbf{T}})\\ &=\tfrac{1}{2}((\mathbf{F}-\mathbf{I})+(\mathbf{F}-\mathbf{I})^{\mathbf{T}})\\ &=\tfrac{1}{2}(\mathbf{SR}+\mathbf{R}^{\mathbf{T}}\mathbf{S}^{\mathbf{T}}-2\mathbf{I})\end{aligned}$$

(9)

This results in a relationship that clearly includes the rotational tensor $\mathbf{R}$. Therefore $\mathbf{E}$ is an appropriate strain tensor when isolating the stretch components of strain within a loaded fracture callus.

2.4 Experimental Application

The detailed protocol evaluating the feasibility of assessing continuous strain distribution on fracture callus cross-sections with an ESPI system was well documented in a recent study [Bottlang et al., 2008]. With a similar experimental approach, newly acquired data are further analyzed here to separate rotation from the deformation gradient tensor as a novel metric for localized anisotropy.

Two adjacent mid-sagittal callus cross-sections of 3 mm thickness were obtained from a single sheep following tibial osteotomy treated by 8 weeks of external fixation (Figure 2). The histologic specimen was stained (toluidine blue) to indicate new callus bone and soft tissue formation. The mechanical hypertrophic non-union specimen was submersed in physiologic saline and kept frozen at −18 °C until testing. On the day of testing, the fracture callus was thawed and mounted horizontally in a custom-built uniaxial compression stage (Figure 3). The specimen ends were rigidly clamped to ensure pure axial compression. Load was applied manually using a micrometer screw and a translation stage (M-461/DS-4F, Newport, Irvine, CA). Load (ELFS-T4M, Entran, Fairfield, NJ) and displacement (M-DVRT-3-SK4, Microstrain, Burlington, VT) sensors acquired global mechanical data at 0.2 N and 1.5 μm resolution, respectively. The entire setup was assembled on a base plate and mounted on an optical table to ensure stable conditions for the Electronic Speckle Pattern Interferometer (ESPI, Q100, Ettemeyer AG, Nersingen, Germany) suspended over the loaded callus arrangement. The ESPI sensor acquired 2D displacements in three-directions at 256×256 individual pixel locations spaced 0.2 mm apart over a 50 mm × 50 mm region of interest. The callus specimen was loaded in quasi-static manner with incremental load steps applied up to a cumulative load of a 5 N. ESPI measurements of the bony cortex, callus, and fracture gap produced a 2D grid pattern map of the displacement field. The rotational angles and principal stretch ratios at each material point throughout the tissue surface were calculated and mapped using a contour function (MATLAB, Mathworks, Inc., Natick, MA).

3. Results

The initial tissue differentiation during fracture healing indicated that new bone was formed directly on both the periosteal (dominant) and endosteal surfaces while fibrocartilage was formed in the interfragmentary gap (Figure 2). Newly formed tissue was identified with toluidine blue staining where collagen orientation had no specific patterns [Chao and Aro,

1997]. Localized rigid body motion of the loaded tissue was quantified by the rotation factor φ associated with the rotation tensor **R** (equation 6), despite any limitations in the boundary conditions. A continuous rotation map was observed on both halves of the callus cross-section in the range of 0.1° to 0.8° (Figure 4) with positive counter-clockwise motion indicated from a horizontal datum. The highest rigid body motion was detected within the interfragmentary gap soft tissue with isolated peak values of 0.8°. All other areas outside of the interfragmentary gap indicated little to no rotation. Simultaneously, deformation was observed to have a minimum stretch or maximum contraction ratio λ_i of 0.98 (2% contraction) within the interfragmentary gap (Figure 5). Beyond the gap region, both rotational and stretch parameters were minimal under uniaxial compressive loading. The fibrocartilage within the interfragmentary gap indicated principal directions of stretch as not aligned with the longitudinal tissue and possibly collagen fiber orientation. This identified region of tissue was associated with a continuous principal direction of 30° to 40° in the medial side (left half) of the callus cross-section (Figures 2 and 6). In other regions of the bony callus and cortex no typical strain patterns or distributions were found (Figure 6).

4. Discussion

In the present study, ESPI acquired strain measurements were made on a highly nonuniform sample with biomaterials ranging from soft tissues to cortical bone. The initial data provided a higher resolution (0.2 mm) and sensitivity (0.01% strain) over the region of interest than typical differential image correlation techniques [Bay, 2001]. Bony tissue located outside of the fracture gap indicated minimal sign of stretch, including little rigid body rotation. The localized rigid body rotation of the interfragmentary gap tissue is presented here as being attributed to the anisotropic nature of constituent collagen fibers, which appear responsive to the applied loading in specific orientations. The length changes as well as localized rotational regions were clearly demarcated and correlated closely to soft tissues visible within the specimen's cross-section (Figure 2). Locations were identified within the gap having rotations with or without coincident stretching. Anisotropy or a directional dependent response was presumed highest when the tissue rotation occurred without stretch. This effect could also be influenced by the regional heterogeneity and the interaction between soft and hard tissues. The location where maximum rotation was observed in the interfragmentary gap also did not match the maximum stretch location. We found that external load-induced rotation and stretch as highly heterogeneous as well as anisotropic relative to that compared with previous studies reporting global (homogeneous) strains for the description of interfragmentary gaps [Bottlang et al., 2008]. Due to a limitation of the scanning capability of ESPI along the specimen edge in this particular implementation, estimated values were not reliable at those boundaries. To resolve this issue, a smoothing algorithm applied to typical edge data will need to be developed in the future. Nevertheless, the maps of the interior area (especially that of the gap region of interest) were shown to be continuous.

With this measurement technique, stretch/rotation calculations, collagen fiber assumptions, and boundary conditions, the estimated gradient tensor $\hat{\mathbf{F}}$ can only partially explain interfragmentary properties. More detailed information on fiber ultrastructure and orientation are needed through histology. Moreover, for a quantitative description of the mechanical behavior associated with mechanotransduction during fracture healing, the relationships between experiments and numerical simulation need to be examined through multiple time steps of healing for any accurate predictions. The resulting maps will provide unique materials characterization for validation with other anisotropic indices [Kohles, 2000] and input for ongoing numerical analysis.

The deformation gradient provides a novel measure of the mechanical response to loading, especially when modeling the interface of soft and hard tissues with highly nonuniform material

properties. Direct measurements with displacement extensometers typically determine strains instead of defining the deformation gradient, despite the fact that strain tensors do not include information about rotation. The approach here has revealed maps characterizing structural anisotropy and heterogeneity of soft tissues within a nonunion fracture. The accuracy of the estimated $\hat{\mathbf{F}}$ as described here was evaluated previously [Peter, 1987] and indicated that $\hat{\mathbf{F}}$ is a statistically unbiased estimate. In load-bearing tissue, the principal direction of stretch will often be aligned with tissue constituent orientation [Carter and Beaupre, 2001]. Since collagen fibers were formed without orthogonal patterns in the callus region, the corresponding principal directions of stretch indicated no expected patterns of orientation. However, in the fibrocartilaginous region of the callus, the formed collagen fibers appear to be associated with the directions of maximum principal stretch, offering some insight toward an indicator of anisotropy. Future work will continue to address accuracy and sensitivity. Specifically, random responses can be added to the gathered surface strain data-sets for each load sequence and the signal-to-noise ratio (SNR) subsequently calculated [Teu and Kim, 2006]. Errors in the stretch and rotation factors due to a range of SNR input will then be separately estimated. In addition, more detailed histological results will facilitate an investigation associating principal stretch directions with both bone and cartilage collagen fiber orientation.

The deformation gradient tensor provided a measure of the subtle deformation within a fracture callus experiencing very low loads. It is especially attractive as it contains information about stretch and rotation. Nonetheless, researchers often report values of strain instead of the full deformation gradient. Here the analytical approach to computing strain from a deformation gradient tensor was demonstrated. In a final twist, one can construct a strain tensor from the deformation gradient, but one cannot do the reverse.

Notations and Conventions

a	Scalar
$\mathbf{a} = a_j$	Vector
$\mathbf{A} = A_{ij}$	Second-order tensor
$^3\mathbf{A} = A_{ijk}$	Third-order tensor
$\mathbf{a} \cdot \mathbf{a}$	Scalar product of two vectors
$\mathbf{a} \otimes \mathbf{a} = \mathbf{P_{ij}} = \mathbf{a_i}\, \mathbf{a_j}$	Dyadic product of two vectors
$\mathbf{A} \cdot \mathbf{a} = A_{ij}\, a_j$	Inner product of a second-order tensor and a vector
$\mathbf{A} \cdot \mathbf{B} = A_{ij}\, B_{jk}$	Inner product of two second-order tensors
$\mathbf{A} : \mathbf{B} = A_{ij}\, B_{ji}$	Double inner product of two second-order tensors
$\mathbf{A^T}$	Transposed matrix
$\hat{a}, \hat{\mathbf{a}}, \hat{\mathbf{A}}$	Estimates of scalars, vectors, or tensors
$\bar{a}, \bar{\mathbf{a}}$	Mean scalar or vector
$\mathbf{A}^{-1}$	Inversion matrix
$\mathbf{A}^{*}, \mathbf{a}^{*}$	Projection tensor or vector
$\lvert \mathbf{A} \rvert$	Determinant of matrix $\mathbf{A}$
$\lVert \mathbf{a} \rVert$	Absolute value of vector $\mathbf{a}$

Acknowledgments

References

Bay BK. Experimental measurement of three-dimensional continuum-level strain fields in trabecular bone. Advanced Experiments in Medicine and Biology 2001;496:181–197.

Bottlang M, Mohr M, Simmon U, Claes L. Acquisition of full-field strain distributions on ovine fracture callus cross-sections with electronic speckle pattern interferometry. Journal of Biomechanics 2008;41 (3):701–705. [PubMed: 18093600]

Chao, EYS.; Aro, HT. Biomechanics of fracture fixation. In: Mow, VC.; Hayes, WC., editors. Basic Orthopaedic Biomechanics. Vol. 2. Lippincott-Raven Publishers; Philadelphia: 1997. p. 317-351.

Carter, DR.; Beaupre, GS. Skeletal Function and Form. Cambridge University Press; Cambridge: 2001.

Claes LE, Heigele CA, Wilke CN, Kaspar D, Seidl W, Margevicius KJ, Augat P. Effects of mechanical factors on the fracture healing process. Journal of Clinical Orthopaedics and Related Research 1998;355S:132–147.

Cowin SC. Tissue growth and remodeling. Annual Reviews of Biomedical Engineering 2004;6:77–107.

Duda GN, Sporrer S, Sollmann M, Hoffmann JE, Kassi J, Khodadadyan C, Raschke M. Interfragmentary movements in the early phase of healing in distraction and correction osteotomies stabilized with ring fixators. Langenbecks Archives in Surgery 2003;387:433–440.

Einhorn TA. Enhancement of fracture-healing. Journal of Bone and Joint Surgery [Am] 1995;77:940–956.

Epari DR, Taylor WR, Heller MO, Duda GN. Mechanical conditions in the initial phase of bone healing. Clinical Biomechanics 2006;21(6):646–655. [PubMed: 16513229]

Erne OK, Reid BR, Ehmke LW, Sommers MB, Madey SM, Bottlang M. Depth-dependent strain of patellofemoral articular cartilage in unconfined compression. Journal of Biomechanics 2004;38:667–372. [PubMed: 15713286]

Gardner TN, Evans M, Kyberd PJ. An instrumented spatial linkage for monitoring relative three-dimensional motion between fracture fragments. Journal of Biomechanical Engineering 1996;118:586–594. [PubMed: 8950664]

Geers MD. Computing strain fields from discrete displacement fields in 2D-solids. International Journal of Solids Structures 1996;33:4293–4307.

Isaksson H, van Donkelaar CC, Huiskes R, Ito K. Corroboration of mechanoregulatory algorithms for tissue differentiation during fracture healing: comparison with In Vivo results. Journal of Orthopaedic Research 2006;24(5):898–907. [PubMed: 16583441]

Kenwright J, Gardner T. Mechanical influences on tibial fracture healing. Journal of Clinical Orthopaedic and Related Research 1998;355S:179–190.

Kohles SS. Applications of an anisotropic parameter to cortical bone. Journal of Material Science: Materials in Medicine 2000;11(4):261–265.

Lanir Y. A structural theory for the homogeneous biaxial stress-strain relationship in flat collagenous tissues. Journal of Biomechanics 1979;12:423–436. [PubMed: 457696]

Lanir Y. Constitutive equations for fibrous connective tissues. Journal of Biomechanics 1983;16:1–12. [PubMed: 6833305]

Marsh DR, Li G. The biology of fracture healing: optimizing outcome. British Medical Bulletin 1999;55:856–869. [PubMed: 10746335]

McCarthy, JM. Geometric Design of Linkages. Springer; New York: 2000.

Park S, O'Connor K, Mckellop H, Sarmiento A. The influence of active shear or compressive motion on fracture-healing. The Journal of Bone and Joint Surgery 1998;80-A(6):868–878. [PubMed: 9655105]

Peters, G. PhD Dissertation. Eindhoven University of Technology; The Netherlands: 1987. Tools for the measurement of stress and strain fields in soft tissue.

Press, WH.; Teukolsky, SA.; Vetterling, WT.; Flannery, BP. Numerical Recipes in C. Cambridge University Press; Cambridge: 1992.

Rodriguez EK, Hoger A, McCulloch AD. Stress-dependent finite growth in soft elastic tissues. Journal of Biomechanics 1994;27:455–468. [PubMed: 8188726]

Sacks MS. Biaxial mechanical evaluation of planar biological materials. Journal of Elasticity 2000;61:199–246.

Teu KK, Kim W. Estimation of the axis of a screw motion from noisy data—a new method based on Plücker lines. Journal of Biomechanics 2006;39(15):2857–62. [PubMed: 16259991]

Umeyama S. Least-squares estimation of transformation parameters between two point patterns. IEEE Transactions on Pattern Analysis and Machine Intelligence 1991;13:376–380.

Appendix

7. Appendix: Estimation of Deformation Quantities from Displacement Fields

The algorithm developed by Peters [1987] was used to estimate the $\mathbf{F}$ at each material point, as defined at the centroid of surrounding markers. The final deformed position vector $\mathbf{x}$ of a point P can be considered as a function of the initial position vector $\mathbf{X}$. The position vector of a neighboring point $\mathbf{x} + \Delta\mathbf{x}$ such as point Q can be approximated to second-order accuracy by a vectorial Taylor-series expansion:

$$\Delta\mathbf{x} = \frac{\partial\mathbf{x}}{\partial\mathbf{X}} \cdot \Delta\mathbf{X} + \frac{\partial^2\mathbf{x}}{\partial\mathbf{X}^2} : \Delta\mathbf{X} \otimes \Delta\mathbf{X} + \mathbf{v}$$

(10)

where $\mathbf{v}$ represents the 'model error' (theoretical discretization or truncation error) due to the fact that $\Delta\mathbf{X}$ and $\Delta\mathbf{x}$ are finite vectors. Equation (10) involves the deformation tensor $\mathbf{F} = \partial\mathbf{x}/\partial\mathbf{X}$ from equation (2) and the gradient deformation tensor $\partial^2\mathbf{x}/\partial\mathbf{X}^2$ of rank three. As $\Delta\mathbf{X}$ and $\Delta\mathbf{x}$ become infinitely small, equation (10) reduces to equation (1). The behavior of the material is characterized by the displacements of a discrete set of points at the surface of the material. To compute the approximated $\mathbf{F}$ from a discrete displacement field, the set of point contributing to $\mathbf{F}$ as the '$\mathbf{F}$ group' has to be defined. An $\mathbf{F}$ group is the set of material markers that surround the central marker in which an $\mathbf{F}$ is to be computed, and is used in the theoretical model to carry out the $\mathbf{F}$ estimation. More markers in an $\mathbf{F}$ group will produce more refined results. Yet, if the distances between the central marker and the surrounding markers become large, the remaining discretization error rises significantly and will adversely influence the computational results. This statement is a generalization of earlier work showing that the spatial composition of a strain group influences the quantitative results [Geers, 1996].

If, from a group of markers, the coordinates are measured for multiple deformed configurations of a body ($i = 1, 2, .., n$), one can calculate the vectors $\Delta\mathbf{X_i}$ and $\Delta\mathbf{x_i}$ which connect one marker $\mathbf{P}$ of the group to the other markers (Figure 1a). The marker $\mathbf{P}$ is called the central marker and is written:

$$\Delta\mathbf{x}_i - \mathbf{F}\Delta\mathbf{X}_i - \mathbf{v}_i = \mathbf{w}_i \text{ for } i \in (1, 2, \ldots, n)$$

(11)

Equation (11) is the starting point for the estimate of $\mathbf{F}$ from measured marker coordinates. The vectors $\Delta\mathbf{X_i}$ and $\Delta\mathbf{x}_i$ are considered to be stochastic due to measurement variability. Based on the maximum likelihood method, this maximum is reached when the differential of the scalar function $\mathbf{J}$:

$$\mathbf{J} = \frac{1}{n}\sum_{i=1}^{n}(\Delta\mathbf{x}_i - \mathbf{F}\Delta\mathbf{X}_i - \mathbf{v}_i) \cdot (\Delta\mathbf{x}_i - \mathbf{F}\Delta\mathbf{X}_i - \mathbf{v}_i)$$

(12)

is minimized (≈ 0) with respect to $\mathbf{v}$ and $\mathbf{F}$. This minimization yields the estimates:

$$\widehat{\mathbf{v}} = \Delta\mathbf{x} - \mathbf{F}\Delta\mathbf{X}$$
$$\widehat{\mathbf{F}} = \mathbf{X}_{01}^{\mathbf{T}} \cdot \mathbf{X}_{00}^{-1} \tag{13}$$

where:

$$\mathbf{X}_{00} = \frac{1}{n}\sum_{i=1}^{n}\Delta\mathbf{X}\otimes\Delta\mathbf{X} - \Delta\overline{\mathbf{X}}\otimes\Delta\overline{\mathbf{X}}$$
$$\mathbf{X}_{01} = \frac{1}{n}\sum_{i=1}^{n}\Delta\mathbf{X}\otimes\Delta\mathbf{x} - \Delta\overline{\mathbf{X}}\otimes\Delta\overline{\mathbf{x}} \tag{14}$$

are called the marker distribution tensors and describe the geometric distribution of the surface markers, providing a metric of the local strain resolution. In addition:

$$\Delta\overline{\mathbf{X}} = \frac{1}{n}\sum_{i=1}^{n}\Delta\mathbf{X}_i$$
$$\Delta\overline{\mathbf{x}} = \frac{1}{n}\sum_{i=1}^{n}\Delta\mathbf{x}_i \tag{15}$$

are the mean vectors of the markers in the reference and deformed configurations, respectively.

In most practical situations, markers are placed on the outer surface of an object. When the outer surface is curved and/or rotates during loading, the marker coordinates have to be measured in 3D, although the distribution of $\mathbf{F}$ on the surface is strictly 2D. Thus a 2D $\mathbf{F}$ is estimated for 3D marker coordinates. For that purpose, two flat planes are defined through a central marker in each of the reference and the deformed configurations, respectively. Consider the reference configuration where a unit vector $\mathbf{N}$ is defined normal to the surface plane at point P. The desired $\mathbf{N}$ can be found from:

$$\mathbf{X}_{00}\mathbf{N} = \lambda_0\mathbf{N} \tag{16}$$

where $\mathbf{X}_{00}$ is the marker distribution tensor in equation (14) and is a symmetrical and semi-positive definite tensor. The desired unit vector $\mathbf{N}$ represents one of the eigenvectors of $\mathbf{X}_{00}$ where the multiplier λ_0 is the corresponding eigenvalue. Further, $\mathbf{N}$ is the eigenvector which corresponds to the smallest eigenvalue λ_0 which is obtained at the maxima or minima as described for equation (12), such that:

$$\mathbf{X}_{11}\mathbf{n} = \lambda_1\mathbf{n} \tag{17}$$

Here, $\mathbf{n}$ is the unit vector normal to the plane at P and λ_1 is the smallest eigenvalue of $\mathbf{X}_{11}$. This procedure then continues throughout the array of surface material points defining the 2D deformation.

It was assumed that all markers lie in the plane just established. Of course this is not always the case, thus the next step is to determine the projection of both of the marker position vectors and the marker distribution tensor on the plane by using the projection tensor (or Projector) such as $(\mathbf{I} - \mathbf{N}\otimes\mathbf{N})$ and $(\mathbf{I} - \mathbf{n}\otimes\mathbf{n})$.

One can show that

$$\mathbf{X}_{00}^* = (\mathbf{I} - \mathbf{N} \otimes \mathbf{N}) \cdot \mathbf{X}_{00} \cdot (\mathbf{I} - \mathbf{N} \otimes \mathbf{N})$$
$$\mathbf{X}_{01}^* = (\mathbf{I} - \mathbf{N} \otimes \mathbf{N}) \cdot \mathbf{X}_{01} \cdot (\mathbf{I} - \mathbf{n} \otimes \mathbf{n}) \tag{18}$$

The $\widehat{\mathbf{F}}$ can be estimated by:

$$\widehat{\mathbf{F}} \cdot \mathbf{X}_{00}^* = \mathbf{X}_{01}^{*\,\mathbf{T}} \tag{19}$$

As $\mathbf{X}_{00}^*$ is singular, a so-called pseudo-inverse is introduced for the determination of $\widehat{\mathbf{F}}$. It follows that we may write $\mathbf{X}_{00}^*$ as:

$$\mathbf{X}_{00}^{*\,-1} = (\mathbf{X}_{00}^* + \mathbf{N} \otimes \mathbf{N})^{-1} - \mathbf{N} \otimes \mathbf{N} \tag{20}$$

$$\widehat{\mathbf{F}} = (\mathbf{I} - \mathbf{n} \otimes \mathbf{n}) \cdot \mathbf{X}_{01}^{*\,\mathbf{T}} \cdot \mathbf{X}_{00}^{*\,-1} \tag{21}$$

In summary, this describes the deformation within a plane described by an array of markers.
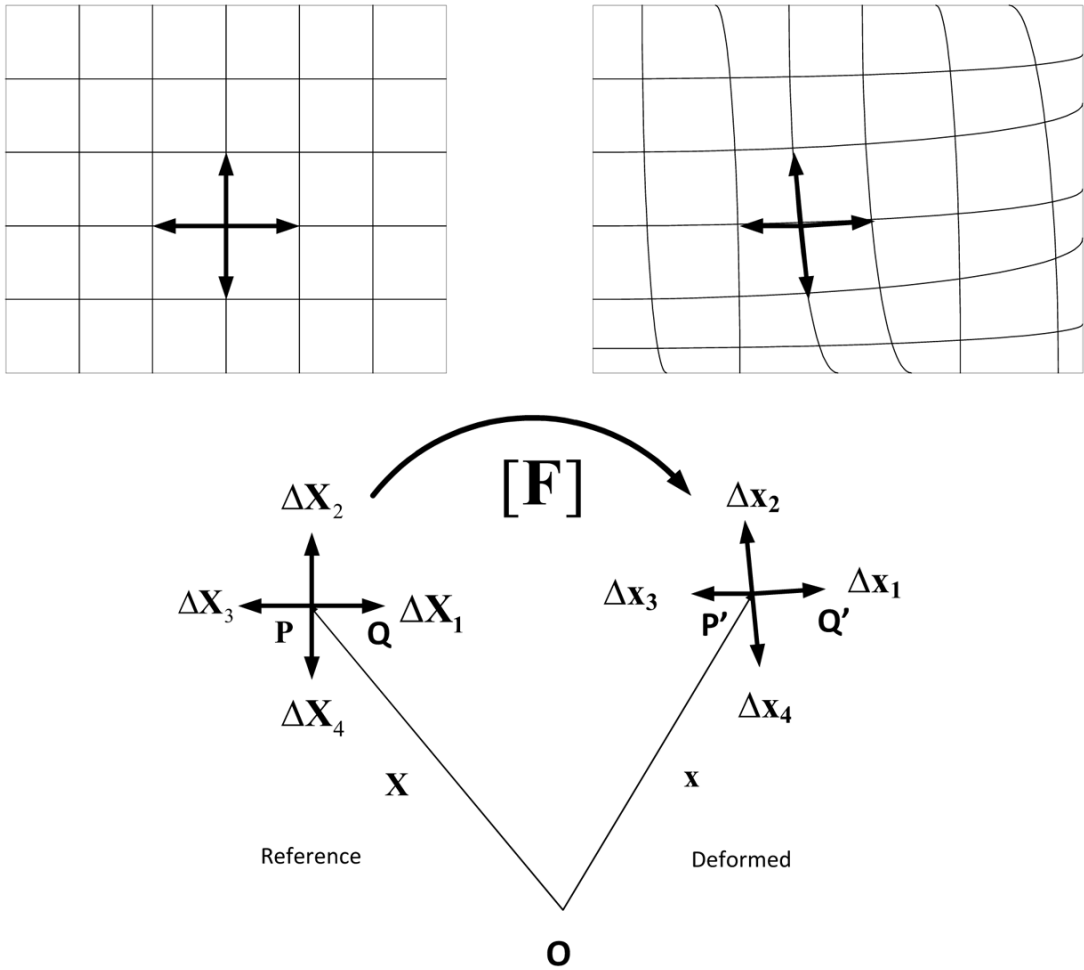
Figure 1.
A generalized 2D surface deformation shown with an intersecting gridwork defining material
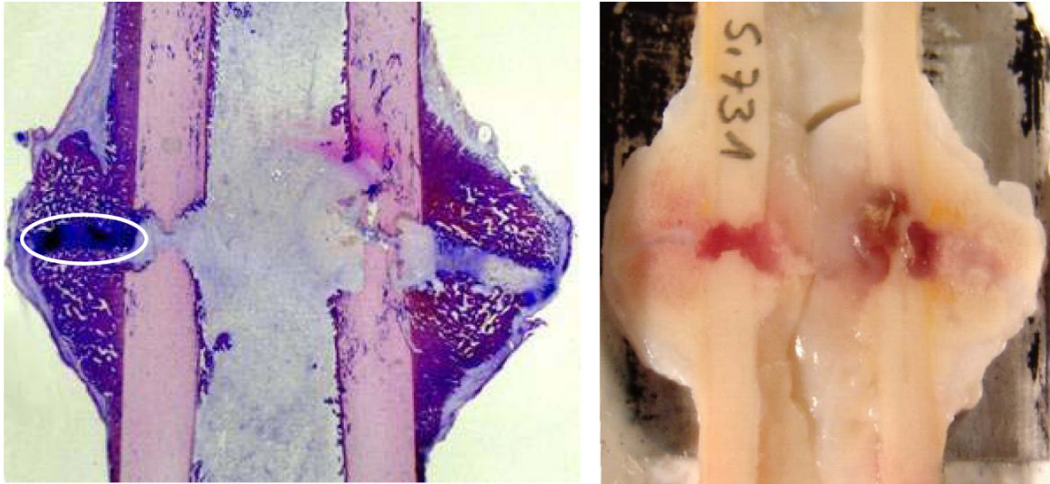markers (P and adjacent point Q) for reference and deformed states.

Figure 2.
Representative histologically stained (toluidine blue) and native mid-sagittal cross-sections of the ovine tibia indicating heterotrophic non-union in both the medial and lateral halves (left and right, respectively). The cortical bone of the tibial cortex, the bony fracture callus, and the soft tissue interfragmentary gap (circled fibrocartilage region) are distinct in each image.
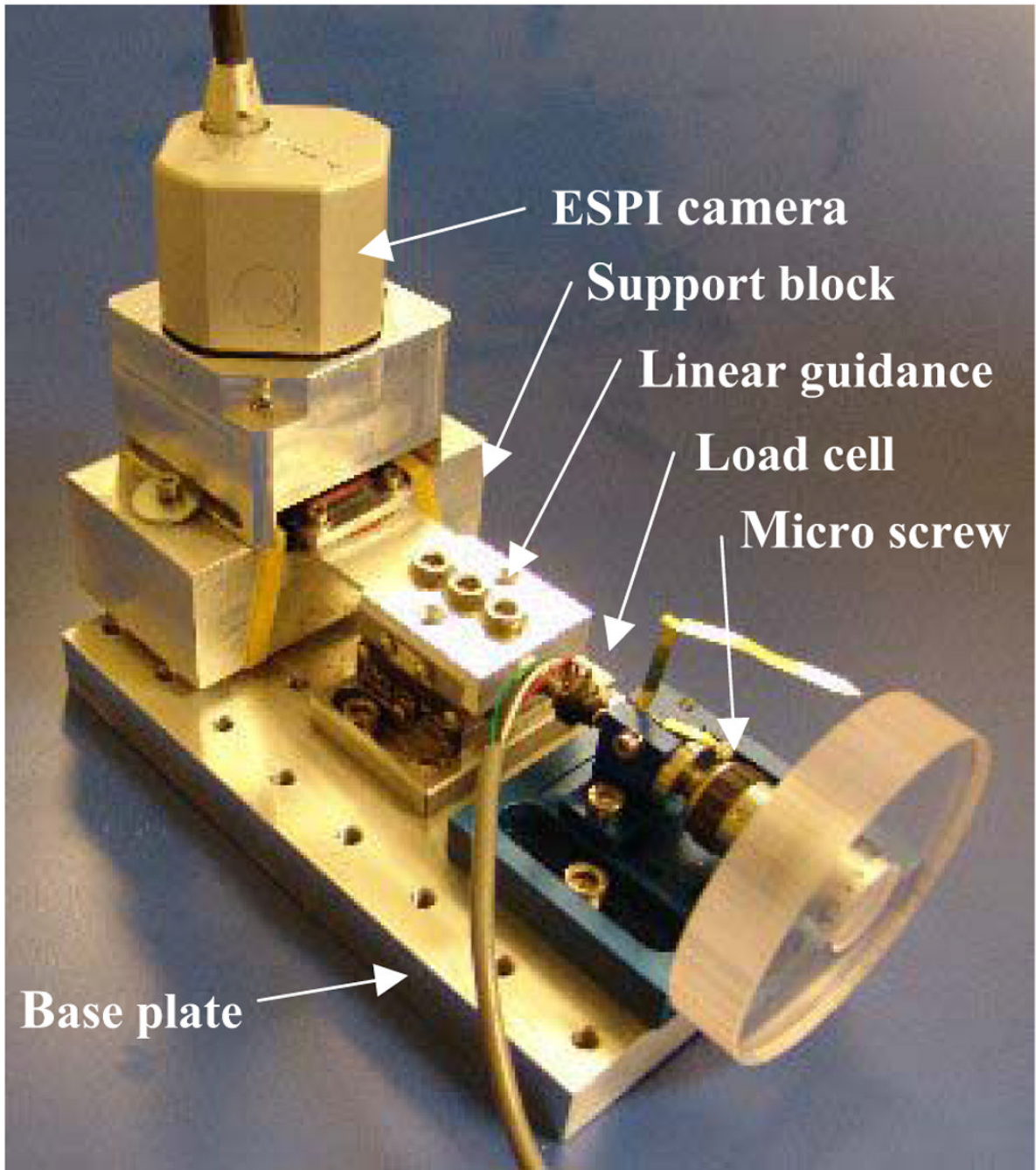
Figure 3.
The custom experimental test setup for planar strain measurement applying the electronic speckle pattern interferometer (ESPI).
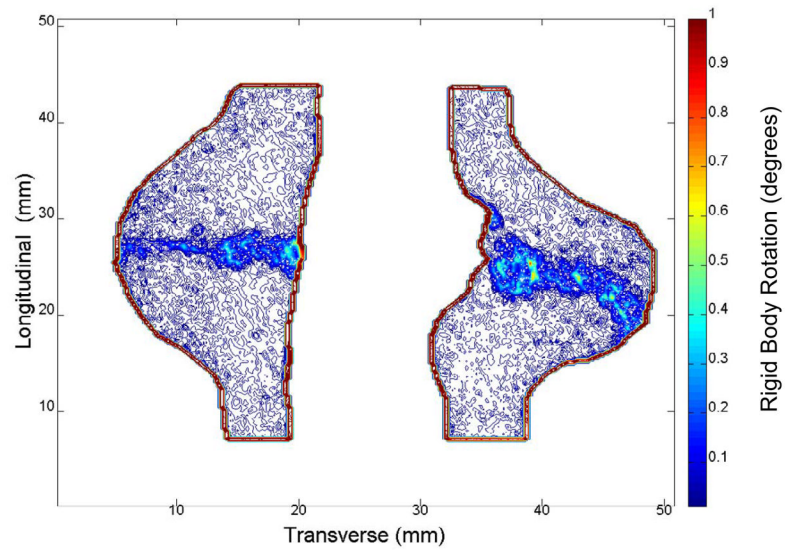
Figure 4.
A map of localized soft tissue rotation φ within the interfragmentary gap of a fracture callus during a 5 N compressive load. Bony rotation during the applied load is effectively zero throughout the cross-section. Rotations are presumed to indicate anisotropic structural properties such as off-axis collagen fiber orientation.
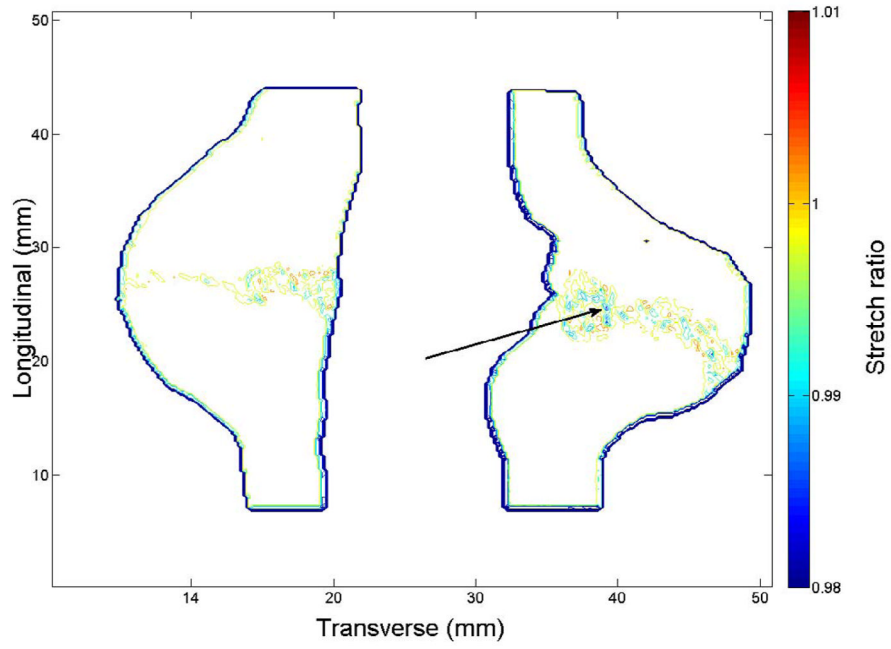
Figure 5.
A map of the localized principal stretch of tissue within and around the interfragmentrary gap. The location at the minimum stretch (maximum contraction) value is indicated by the arrow.
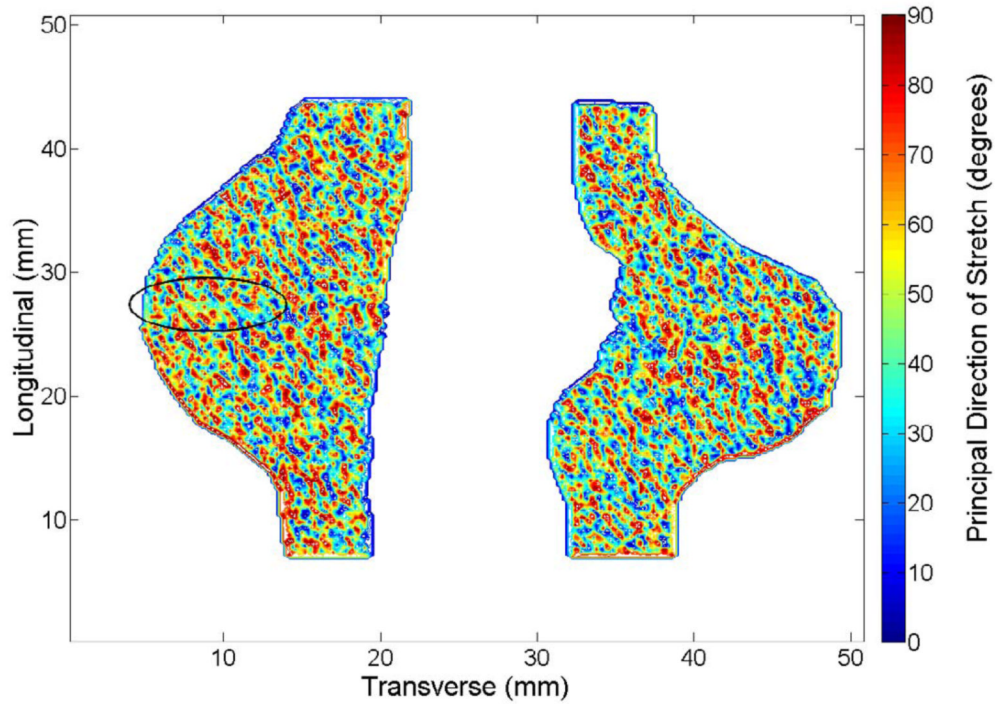
Figure 6.
A map of the localized principal direction of tissue stretch throughout the fracture region including the interfragmentrary gap. The circled region indicates tissue ultrastructure not contiguously aligned with the longitudinal principal direction of loading (anisotropy causing both rotation and minimal stretch). Here, the regions closer to darker blue display a more horizontal direction of the principal stretch (0°). Regions closer to reddish-brown in color indicate stretches more vertically oriented (90°).